MEDDOCS Open Access Publisher

ISSN: 2640-1223

Journal of Veterinary Medicine and Animal Sciences

Open Access | Research Article

MRI-Guided Focused Ultrasound Robotic System for Preclinical use

T Drakos[1]; M Giannakou[1]; G Menikou[2]; A Filippou[2]; N Evripidou[2]; K Spanoudes[2]; L Ioannou[3]; C Damianou[2]*

[1]R & D, MEDSONIC LTD, Limassol, Cyprus.

[2]Electrical Engineering Department, Cyprus University of Technology, Limassol, Cyprus.

[3]Radiology Department, Ygia Polyclinic, Limassol, Cyprus.

***Corresponding Author(s): Christakis Damianou**

Cyprus University of Technology, Electrical Engineering Department, Cyprus University of Technology, 30 Archbishop Kyprianou Str, 3036 Limassol, Cyprus.

Tel: 0035725002039, Fax: 0035725002849;

Email: christakis.damianou@cut.ac.cy

Received: Sep 29, 2020

Accepted: Feb 16, 2021

Published Online: Feb 19, 2021

Journal: Journal of Veterinary Medicine and Animal Sciences

Publisher: MedDocs Publishers LLC

Online edition: http://meddocsonline.org/

Keywords: MRgFUS; HIFU; Preclinical; Robotic system; Rabbit ablation.

Abstract

Objectives: A Magnetic Resonance Image (MRI) guided focused ultrasound system with a robotic device with 4 Degrees of Freedom (DOF) has been developed. The device has been developed for preclinical use on animals and can fit in commercial MRI scanners up to 7 T. The transducer operates at 1.1 MHz and hence can be used for deep tissue ablation, drug delivery or opening of the blood brain barrier.

Methods: MRI compatibility of the robotic device and the transducer was evaluated successfully. The accuracy of the robotic device was tested using a special structure attached to the robot and using a digital caliper. The device was evaluated in an agar-based phantom, in excised porcine loin tissue as well as *in vivo* thigh tissue of a rabbit model, in a laboratory setting and MRI environment. Its functionality was evaluated in terms of Magnetic Resonance (MR) thermometry providing near real-time temperature feedback.

Results: The ability of the ultrasonic transducer was confirmed by successfully creating discrete and overlapping thermal lesions. The transducer creates uniform cigar shaped lesions. The *in vivo* ablation procedure resulted in *in situ* tissue coagulation necrosis without damaging intervening tissues. The procedure was proven safe without any adverse effects thus not affecting the welfare of the animal.

Conclusions: The proposed system fits in all MRI scanners and offers accuracy of motion close to 0.11 mm. Because of its size it can be used on small animals. In the future it can be scaled up for use in humans for abdominal targets.

Cite this article: Drakos T, Giannakou M, Menikou G, Filippou A, Evripidou N, et al. MRI-Guided Focused Ultrasound Robotic System for Preclinical use. J Vet Med Animal Sci. 2020; 4(1): 1049.

Introduction

The first Focused Ultrasound (FUS) prototype was built in 1940 [1] and the general technology existed in an experimental setting for over 70 years. FUS can be focused on a targeted point to induce a rise in temperature between 60-80 °C. As a result, thermal tissue coagulation necrosis is achieved. Each sonication heats only a small focal target, so multiple sonications, must be used to ablate an entire target area [1]. Due to the propagation mechanism of ultrasound, this technique must be performed with caution near nerves and bones.

Only recently has this technology been employed for approved clinical applications. Two FUS devices are currently available for prostate cancer therapy using ultrasound imaging guidance: Ablatherm (EDAP TMS SA, Vaulx-en-Velin, France) [3] and Sonablate (Focus Surgery Inc., Indianapolis, IN, USA, now called SONACARE) [5].

Recently, Magnetic Resonance Guided Focused Ultrasound (MRgFUS) has been introduced due to a better ability to plan and monitor treatments in real-time [6]. This technique is approved by the Federal and Drugs Administration (FDA) for fibroid ablation. The InSightec (Haifa, Israel) systems have been deployed very fast in the last decade in other applications such as the treatment of prostate cancer [7], breast cancer [8], liver [9] and for pain palliation of bone metastases [10]. Recently, Insightec developed a transcranial MRgFUS system which eliminates non-invasively essential tremor [11]. This application is becoming the gold standard and establishes FUS as a safe, effective and non-invasive treatment modality. Therefore, the number of research institutions involved in the area of MRgFUS is growing rapidly. Thus, there is an unmet need for research institutions for affordable and functional preclinical MRgFUS robotic systems in order to explore new applications in MRgFUS.

There is an evolution of MRgFUS preclinical systems in the last decade. Chopra et al. [12] developed an MRI three-axis positioning system that delivers focused ultrasound in small animals for high-throughput preclinical drug delivery studies. This robot is not commercially available.

Another company that developed an MRgFUS system for small animal experiments is the French company Image Guided Therapy (Pessac, France) [13]. Image Guided Therapy uses phased arrays to move the focus and therefore, this technology is very expensive, and not cost effective for small animals.

Another positioning device is the fully MR-compatible robotic assistance system InnoMotion (InnoMedic GmbH, Herxheim, Germany) which was originally designed for MR-guided interventions with needles [14]. This system has five pneumatically driven degrees of freedom and can be moved over a wide range within the bore of the magnet. The robotic system was combined with a fixed-focus ultrasound transducer. The size of this system is large, thus the price of this system is high. To our knowledge the sales of this device were minimal.

The Canadian company FUS instruments [15] developed a 2-axis positioning device, with all moving parts immersed in water. This device was developed for hyperthermia or Blood Brain Barrier (BBB) opening and is fully compatible with all preclinical Bruker BioSpec small bore high-field MRI systems. A 3-axes positioning device which upon customization can be used for the same treatments, has also been developed and is fully compatible with clinical MRI systems of all manufacturers. Their product range also comprises non-MR guided systems, including a 3-axes stereotactic positioning system for brain sonications with real-time acoustic feedback for exposure monitoring, as well as a FUS system for brain sonications combined with microscopy imaging.

The Korean company Alpinion [16] has been the first to develop a three-axes positioning control device, which has gained approval for animal treatment in Korea. The ultrasound guided device is integrated with a treatment table and water degassing system and can be used for a variety of applications including ablation, histotripsy, cavitation studies, drug delivery and BBB opening on animals weighing up to 50 lbs.

The newly founded Danish company TooSonix [17], has manufactured a high frequency ultrasound system for small animal dermatology research. The system uses two transducers operating at 20 MHz and focusing at 2.7 mm. The device is combined with a microscope, providing visual feedback of the treated area, and is currently undergoing process for clinical approval for dermatologic uses.

The American company Verasonics [18] has collaborated with leading transducer manufacturer Sonic Concepts (Washington, USA), for the development of an ultrasound guided system for preclinical use. The system provides linear movement in 2 axes and is integrated with 3 different transducers, thus providing a range of frequencies. The system exists in two sizes, depending on its deliberate use with small or large animals.

The proposed device can be applied for preclinical use on small animals (mice, rats, rabbits, cats and small dogs). It is MR compatible and provides movement in 4 DOF (3 linear and 1 angular). The device has been entirely developed using 3D printing technology. The inclusion of an angular stage offers improved maneuverability thus avoiding critical structures (bones or nerves or arteries).

Materials and methods

Robotic system

Mechanical design of the positioning device

The entire robotic system was developed using the software MicroStation (V8, Bentley Systems Inc.). After completion of the design, drawings of the individual parts were sent to an industrial 3D printer (FDM400, Stratasys, 7665 Commerce Way, Eden Prairie, Minnesota, 55344, USA) for production. This 3D printer produces parts made out Acrylonitrile Butadiene Styrene (ABS).

The positioning device provides movement in 4 DOF, 3 linear axes (X, Y, Z) and 1 angular axis (Θ). Each axis is driven by a piezoelectric ultrasonic motor (USR30-S3, Shinsei Kogyo Corp., Tokyo, Japan). The dimensions of the device are 57 cm in length, 21 cm in width and 11.5 cm in height. Due to its small dimensions, the device can be placed on the table of any conventional MRI scanner up to 7 T. Due to the thickness of the device, a 5 cm bed mattress is required. The positioning device has a motion range of 29 mm on the X axis, 31 mm on the Y axis, 39 mm on the Z axis and ±90° on the Θ axis. The weight of the positioning device is approximately 5 kg, providing ease of transfer.

The linear axes use a jack-screw mechanism to convert rotational motion into linear. The jackscrew, attached to the X axis frame and connected with the X axis motor, is designed with a pitch of 4.8 mm thus, providing displacement of 4.8 mm in the X axis for every 360° rotation. The Y axis uses an identical mechanism, but with its frame modified so it can be attached

on the frames of the X and Z axes. For the Z axis, rotational motion from the motor is transferred to the jackscrew through 3 linearly coupled spur gears; the first gear coupled on the motor and the third gear mounted on top of the Z axis jackscrew. The Z axis frame is connected to the frame of the Θ axis. The Θ axis motor was coupled to a dual gear mechanism with a motion ratio 9:1 thus, providing 1 complete revolution of the Θ axis for every 9 motor revolutions. A front cover was developed with a coupling designed to connect the transducer shaft to the Θ axis. To ensure linear motion accuracy, optical encoders (EM1-0-500-I, US Digital Corporation, Vancouver, WA 98684, USA) with a resolution of 500 lines per inch were used on all axes providing linear movement. Angular motion accuracy was assured using an optical encoder (EM1-2-2500-I, US Digital Corporation, Vancouver, WA 98684, USA) with a resolution of 2500 lines per one revolution. The encoder output is connected to the counter input of a data acquisition card (USB 6251, National Instruments, Austin, USA).

The positioning mechanism was fixed on the base of the device. Water is needed as an ultrasound transmission media, hence a water container was located on the front of the device and attached to the base using a rigid coupling. A transparent film is used to cover the acoustic opening of the water container, therefore allowing for propagation of ultrasound through the water into the tissue. All the mechanisms were enclosed by covers for aesthetic purposes. Figure 1A shows the computer-aided design (CAD) of the complete robotic system (interior). Figure 1B shows the cross section of the device as placed on the MRI table whereas Figure 1C shows the completed robotic system including the cover.

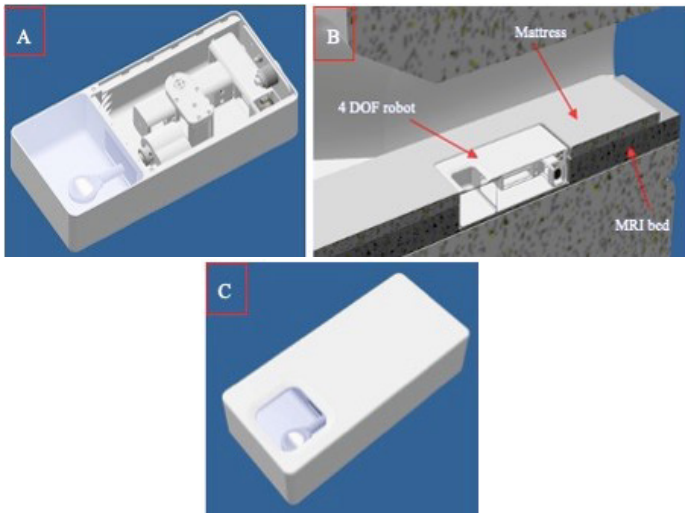

Figure 1: (A) Complete CAD design of the robotic system showing the interior of the device, (B) Cross section of the device in the MRI (isometric view), (C) Complete design of the robotic device including the cover.

Software

The positioning device can be controlled through a developed program written in C # (Visual Studio 2010 Express, Microsoft Corporation, USA). The software provides a user- friendly interface with the following features: a) communication with the MRI, b) manual or automatic movement of the 4 axes, c) MR thermometry and d) ultrasound exposure control (frequency, power, sonication time etc.).

Robot drivers

The rotation of each ultrasonic motor is controlled by a driver (D6030, Shinsei Kogyo Corp., Tokyo, Japan) that operates using a DC power supply (24 V, 6A). The drivers are located inside a metallic enclosure that was placed outside the MRI room.

FUS system

The FUS setup is composed of a MR compatible spherically focused ultrasonic transducer (MEDSONIC, Limassol, Cyprus) operating at a frequency of 1.1 MHz. The transducer has a radius of curvature of 10 cm and a diameter of 5 cm. The ultrasonic transducer is operated by an RF generator (AG Series Amplifier, model AG1012, T&C Power Conversion Inc.) which is controlled by the software.

Motion accuracy

The motion accuracy of the 4 DOF robotic device was evaluated using a digital caliper (ROHS NORM 2002/95/EC) and a specially designed set-up. The set-up was designed in a way that the caliper could be mounted and stabilized on the transducer holder, thus offering an accurate measurement of the linear motion of the robotic device. The set-up consists of individual parts made out of ABS material printed with a 3D printer (F270, Stratasys, 7665 Commerce Way, Eden Prairie, Minnesota, 55344, USA). The accuracy of the motion was evaluated in the X, Y and Z axes as shown on Figure 2A and 2B (only X and Y are shown). A digital angle caliper (Model HG00962B, Powerfix, OWIM GmbH & Co. KG, Germany) was mounted on the Θ axis in order to measure the accuracy of the angle as shown on Figure 3.

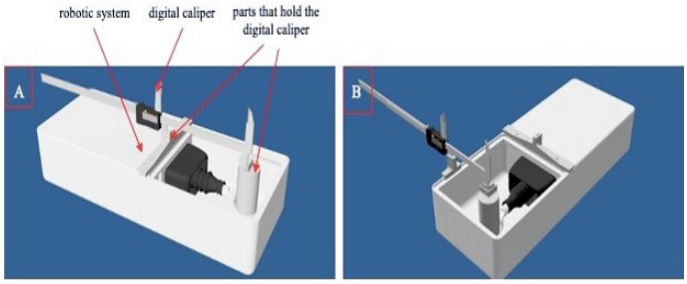

Figure 2: (A) Evaluation of the motion of the robotic device in the X axis. (B) Evaluation of the motion of the robotic device in the Y axis.

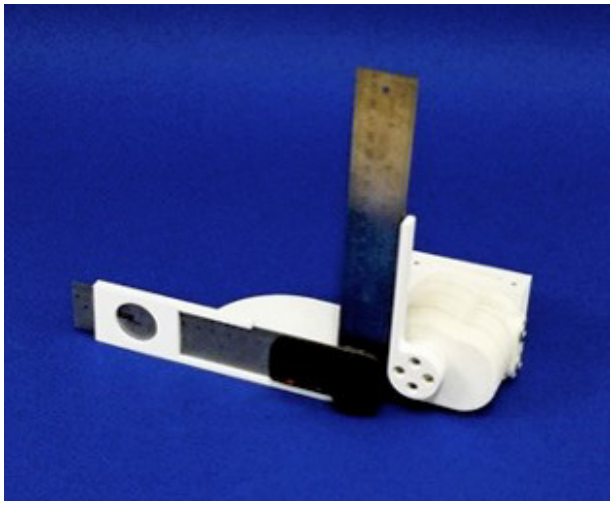

Figure 3: Design used for the measurement of motion accuracy in the Θ axis.

The robotic device was controlled and moved in forward and reverse directions in X, Y and Z axes in increments of 1, 5 and 10 mm, using the software. Accuracy of angular motion was achieved by rotating the Θ axis in angle increments of 5 and 10 degrees (°) in a clockwise (CW) and counterclockwise (CCW) direction. The motion accuracy of the robotic device was evaluated in each direction, by iterative comparison of the distance as set by the software (intended) and the distance as measured by the caliper (measured). Time taken to travel the distance was also measured, hence, the velocity of motion in each linear axis was calculated.

Movement of the robotic device along the axes, was used to evaluate the ability of the device to create lesions in a grid pattern. Experiments were conducted in the laboratory setting and in the MR environment.

Experiments in gel phantoms, *ex-vivo* porcine tissue and *in vivo* rabbit model

In order to check the functionality and the repeatability of the positioning device and to evaluate the performance of the transducer, experiments were performed in agar-based phantoms, freshly excised porcine loin tissue and *in vivo* rabbit thigh tissue. The fresh excised tissue was homogeneous with minimal fat, purchased from a local butcher shop before the execution of the experiment. The agar-based phantom was developed in the laboratory to mimic the absorption of tissue with a concentration of 6 % w/v agar (10164, Merck KGaA, Darmstadt, Germany) and 30 % v/v evaporated milk (Nounou, Friesland Campina, Marousi, Greece). The rabbits were purchased from an accredited farm. All *in vivo* experiments were approved by the authorities of the Veterinary Services, Ministry of Agriculture, Cyprus.

MR compatibility

The MR compatibility of the FUS system was evaluated in a 1.5 T MR system (Signa, General Electric, Fairfield, CT, USA) using GPFLEX coil (USA instruments, Cleveland, OH, USA).

The Signal to Noise Ratio (SNR) in a specific location in the agar-based phantom for transducer compatibility was measured under various conditions (no hardware, motor activation or not, transducer activation or not).

A method in the National Electrical Manufacturers Association (NEMA) standard [19], was used to measure the SNR in the agar phantom for different configurations. A measurement Region of Interest (ROI) of at least 75 % of the area of the signal-producing volume of the phantom image was selected. The SNR was calculated by dividing the mean signal (S_{image}) of that ROI from the standard deviation of the same area (in pixels) in the background of the image ($SD_{background}$) (noise) as shown in the following equation (1).

$$SNR = \frac{S_{image}}{SD_{background}} \quad (1)$$

The transducer performance was evaluated using T1 Weighted-Fast Spoiled Gradient (T1-W FSPGR) sequence with the following parameters: Repetition time (TR)=40 ms, echo time (TE)=19 ms, field of view (FOV)=21 cm, matrix=128 x 128, flip angle=30°, Number of excitations (NEX)=1 for various conditions. The background image was taken with both the transducer and amplifier deactivated. Images were then taken for activation of the amplifier and activation of the transducer for a time range 12-60 s. Hence, the SNR was calculated for each of the cases.

The MR compatibility of the robotic system was assessed using T2-Weighted Fast Relaxation Fast Spin Echo (T2-W FRFSE), FSPGR and Echo Planar Imaging (EPI) sequences for various conditions. We have evaluated these 3 sequences because the first is used for high-resolution imaging and the other two for MR thermometry. The background image was taken with the MR phantom alone. Images were then taken for the robotic device close to the phantom (no cables attached), the device with cables attached (electronic system deactivated) and the device with the electronic system ON. Therefore, the SNR was calculated for each of the cases.

All components (piezoelectric motor, optical encoder and transducer) require the use of electricity during activation hence, according to the American Society for Testing and Materials (ASTM) standards (F2503, F2052, F2213, F2182, F2119), the device is classified as MRI-conditional.

Evaluation of the FUS system in gel phantoms and *ex vivo* tissues

The transducer was evaluated in laboratory and MRI setting for its ability to provide increased temperature and create lesions at the focal point. A specially designed phantom/ *ex-vivo* tissue plastic (ABS) holder was developed to fit in a water tank with the transducer placed at the bottom of the holder. This structure was developed so that a thermocouple (HH806AU, Omega Engineering, USA) could be placed every 5 mm within the target, to provide measurements of temperature increase at set distances along the target. Figure 4 shows the design of the developed holder. With this design, the focal point of the transducer could be easily located and a profile of the temperature increase in near field and far field was taken. The thermocouple was inserted at different locations with 5 mm steps. A constant value of acoustical power of 11 W and a sonication time of 60 s were used at every spatial step, in order to locate the focal depth of the transducer inside the *ex vivo* tissue. After location of the focus, higher values of acoustical powers were used for tissue ablation. Figure 5A shows the axial T2-Weighted Fast Spin Echo (T2-W FSE) MR image of the set up whereas, Figure 5B shows the coronal plane of the same setup.

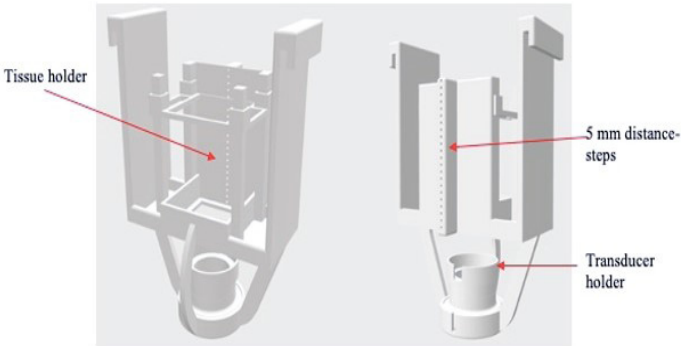

Figure 4: Schematic of plastic holder used for experiments on agar based phantom or excised animal tissue.

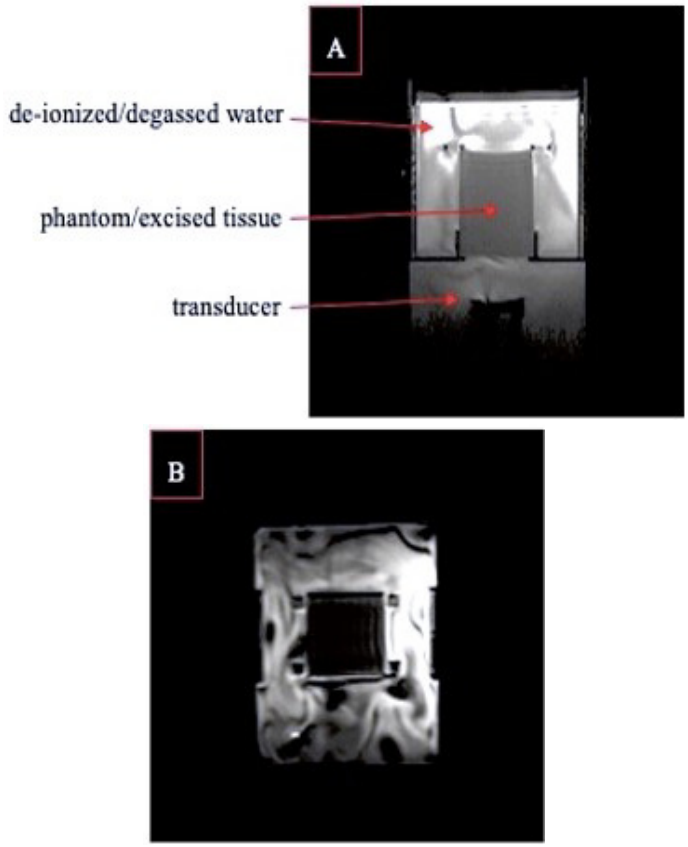

Figure 5: (A) T2-W FSE image (axial plane) of the experimental set-up for the evaluation of the transducer, (B) T2-W FSE image (coronal plane) of the experimental set-up.

MR Thermometry

MR thermometry data were produced using the proton resonance frequency shift equation which is described in great detail in Menikou and Damianou [20]. The equation relates the measured phase with the temperature elevation (ΔT) This relationship is given by:

$$\Delta T = \frac{\varphi(T) - \varphi(T_0)}{Y \alpha B_0 TE} (2)$$

where ϕ(T) and ϕ(T_0) are the phases at a starting and final temperature T and T_0 respectively, γ is the gyromagnetic ratio, α is the proton resonant frequency shift coefficient (0.01 ppm/°C), B_0 is the magnetic field strength and TE is the echo time. The SPGR pulse sequence was used to extract the MR thermometry maps with a 2 s temporal resolution with the following parameters TR=38.5 ms, TE=20 ms, FOV=21 cm, matrix=128 x 128, flip angle=20°, NEX=1.

Evaluation of the FUS system in *in vivo* rabbit model

The FUS system was evaluated in laboratory and MRI setting to assess its safety and efficiency in ablating healthy living thigh tissue on a rabbit model (n=20) and to identify any adverse effects. Upon transfer to the laboratory premises, the rabbits underwent injectable Ketamine (0.15mg/kg) and Medetomidine (0.5 mg/kg) anaesthesia and their thighs were depilated (VEET, Reckitt Benkiser, UK). Prior to FUS exposure, an X-ray system (IMS001, Shenzen Browiner Tech Co. Ltd) was used to acquire images of the thigh to allow calculation of muscle area so as to avoid ultrasonic exposure of the bone. The animal was then placed on the robotic device, with the thigh area intended for ablation, immersed in the water above the transducer. Figure 6 shows the animal placement on the robotic device. Motion of the robotic device in different grid patterns was used to create discrete and overlapping lesions. Different values of acoustical power and sonication time were used to examine their effect on tissue coagulation necrosis. Vital signs (heart rate, respiratory rate) and urination were regularly monitored throughout the procedure. Upon completion of the FUS exposure, the rabbits were humanely euthanized with intracardial injection of T-61 (MSD Animal Health, USA) and *ante mortem* dissection was used to confirm tissue necrosis.

Figure 6: Placement of the rabbit on the robotic device for in vivo thigh ablation.

Results

Motion Accuracy

Intended versus measured distance for forward and reverse movement in the X axis is shown on Figure 7A and 7B respectively. The percentage error at different distance steps and the speed of motion in all axes are summarized on Table 1.

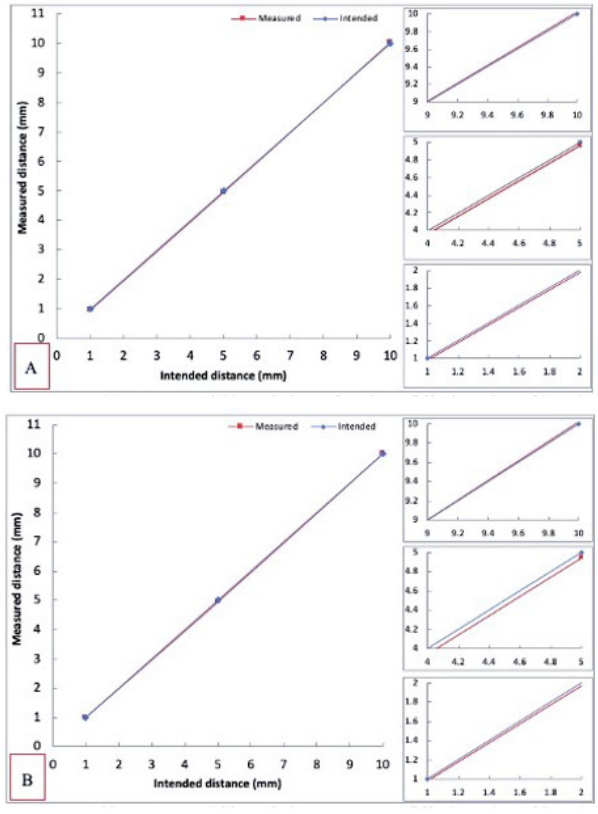

Figure 7: (A) Measured distance versus intended distance for the X axis forward motion (left) and zoomed areas of the graph (right), (B) Measured distance versus intended distance for the X axis reverse motion (left) and zoomed areas of the graph (right).

Table 1: Percentage error at different distance steps and directions on all axes.

Direction	Axis	Step			Speed
		1	5	10	
		Error (%)			
Forward	X	2.15	0.75	0.24	1.56 mm/s
	Y	5.65	2.16	0.48	3 mm/s
	Z	0.7	2.13	1.17	7.8 mm/s
CW	Θ	-	2.6	2	40.4 °/s
Reverse	X	1.45	1.1	0.22	1.67 mm/s
	Y	6.05	2.14	0.71	3.1 mm/s
	Z	0.35	2.12	0.9	7.76 mm/s
CCW	Θ	-	1	0.45	40.8 °/s

MR compatibility

Figure 8 shows the MR images acquired on coronal plane for different activation conditions of the transducer while Figure 9 shows the SNR as calculated from the raw data. It can be seen that SNR is decreased when the amplifier is turned ON. There is minimal difference in the SNR at different time intervals. Figure 10 shows the MR images acquired for different activation conditions of the robotic device using T2-W FSPGR sequence. Figure 11 shows the normalized SNR of the robotic device for the different activation conditions and different MR sequences. There is a decrease of SNR in all sequences upon connection of the robot. There is another decrease upon powering the robotic device. T2-W FSPGR provides the biggest drop in SNR among the three different MR sequences. EPI and FSPGR have approximately the same values of SNR for phantom only, robot in bore and robot connected. However, EPI resulted in a lower SNR value than FSPGR when the robot was activated.

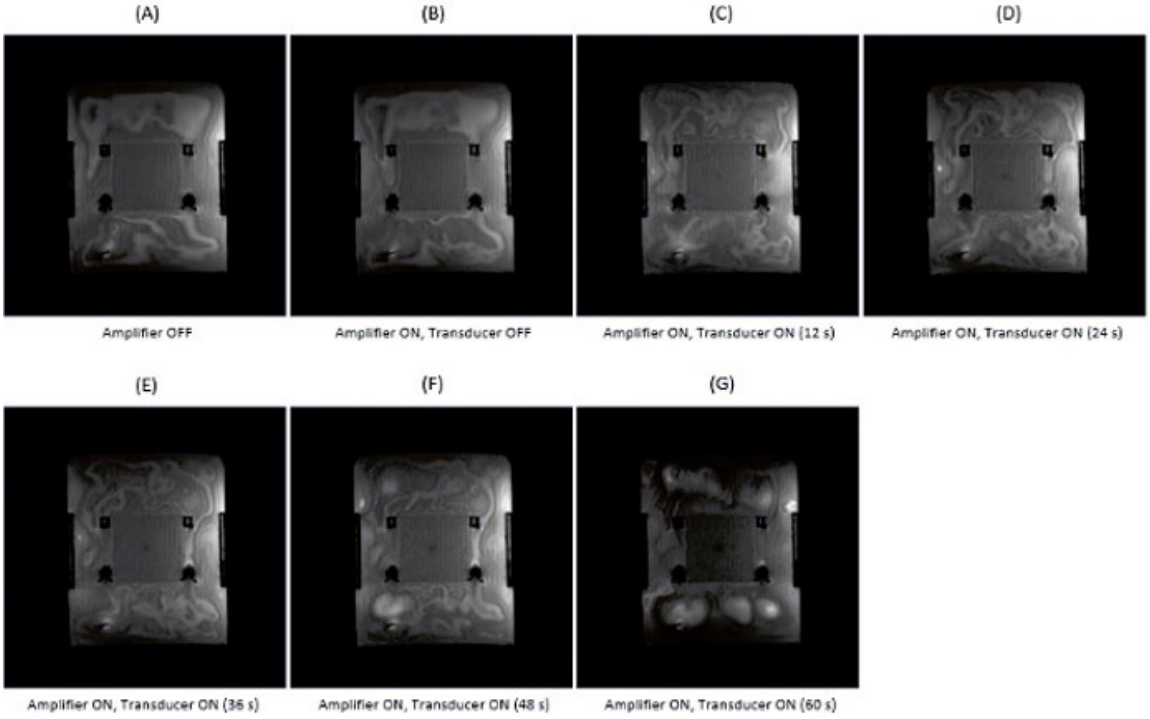

Figure 8: MR images acquired on coronal plane with T1-W SPGR for different transducer activation conditions.

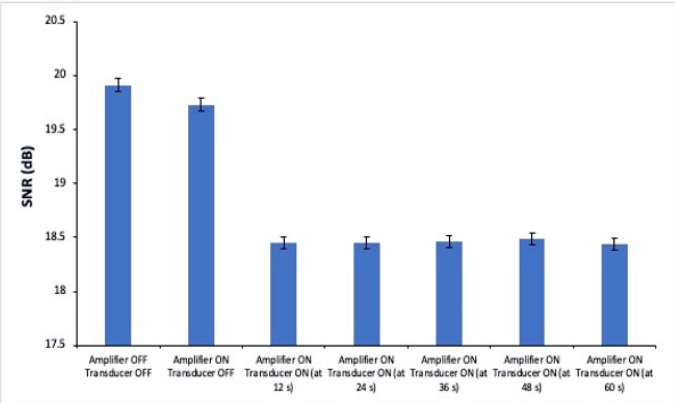

Figure 9: SNR using T1-W SPGR sequence measured for different activation conditions of the transducer.

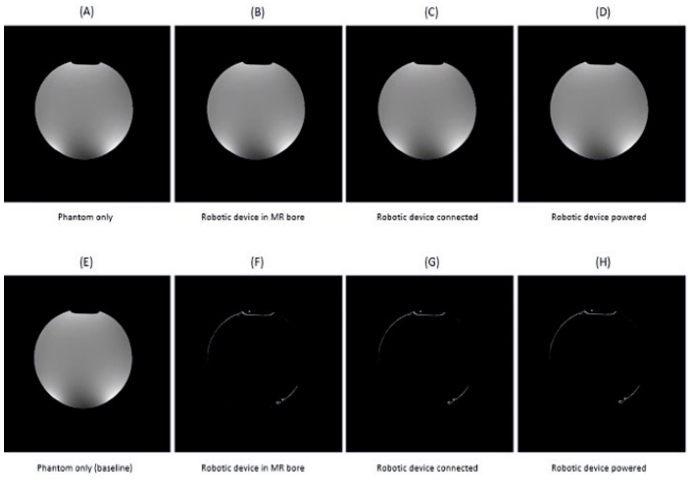

Figure 10: T2-W FSPGR MR images (top) obtained for various system activation conditions and their corresponding differences (bottom).

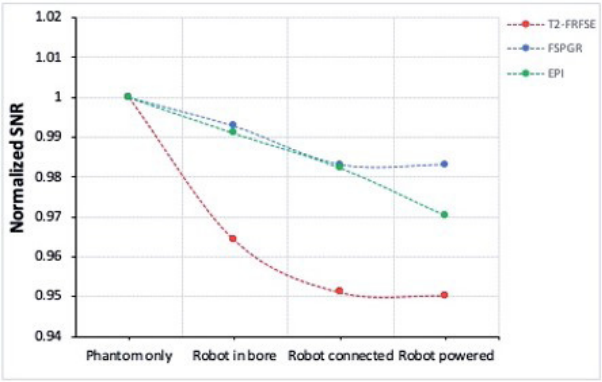

Figure 11: SNR for three MR imaging protocols with the system in different configurations.

Temperature profiles

Figure 12 shows the temperature change versus the distance of the thermocouple along the *ex vivo* tissue. A constant value of acoustical power of 11 W for a sonication of 60 s was used in 5 mm distance increments in order to measure the temperature increase at every location and find the focus of the transducer. The expected focal depth of the transducer was at 30 mm but was shifted to 15 mm deep in the tissue.

After locating the focal point, an increased value of acoustical power of 48 W was used to ablate the tissue for 20 s at the focal point of 15 mm. Figure 13 shows the rate of change of temperature at the focus. The sonication resulted in a temperature increase of 58 °C thus resulting in tissue ablation creating a 30 mm long lesion.

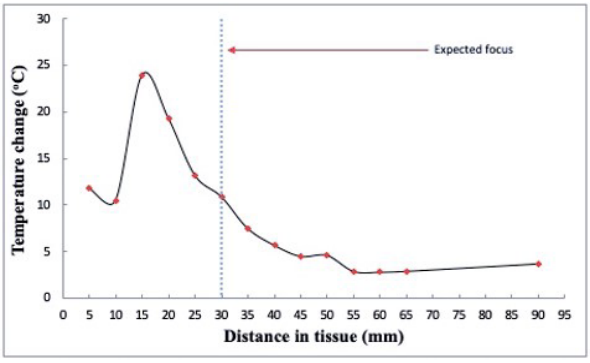

Figure 12: Temperature change versus depth in the excised tissue (pork), frequency 1.1 MHz, acoustical power 11 W, sonication time 60 s.

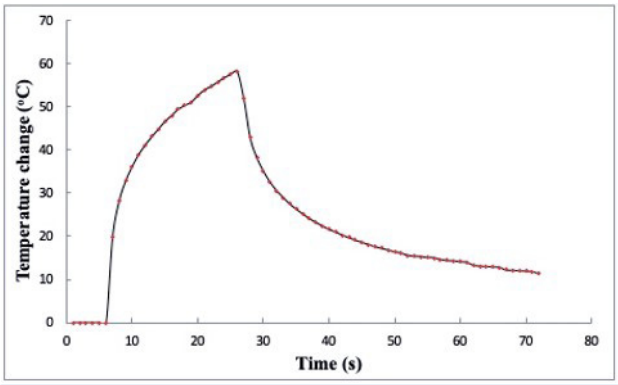

Figure 13: Temperature change versus sonication time for the transducer with frequency 1.1 MHz at acoustic power of 48 W, sonication time 20 s and focal depth of 15 mm.

MR evaluation in *ex vivo* tissue

The transducer was evaluated inside the MRI environment for a sonication with acoustical power of 63 W for 30 s. MR thermometry maps were acquired during sonication. Figure 14 shows the acquired thermal map. From the map, the increase of temperature can be observed during the duration of sonication. Large increase of temperature was acquired at the end of the sonication, resulting in the formation of a lesion.

Figure 15A and 15B show the MR image of the formed lesion acquired on axial and coronal plane respectively. The lesion was 3 mm wide and 32 mm long as measured from the MRI image. The tissue was sliced, and the lesion dimensions were measured using the caliper. Figure 16 shows the sliced tissue with a lesion that was 5.4 mm wide and 44 mm long.

Movement of the robotic device was used to provide lesions in a 3 x 3 array pattern on excised tissue. Sonication was performed at acoustical power of 74 W at a focal depth of 4 cm and sonication times of 40 s and 50 s. Figure 17A shows the lesions formed at the focal point at a plane perpendicular to the beam whereas figure 17B shows the formed lesions at a plane parallel to the beam. Lesions in the first two rows were produced for sonication of 40 s. The bottom row was produced for sonication of 50 s. Lesions formed at 40 s had an average diameter of 6.1 mm and an average length of 36.24 mm. Lesions formed at 50 s had an average diameter of 7.1 mm and an average length of 42.2 mm.

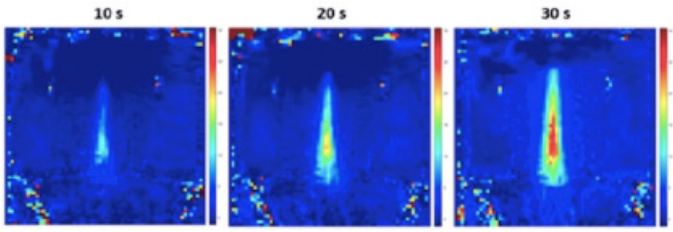

Figure 14: Temperature maps using FSPGR on axial plane recorded for acoustical power of 63 W and sonication time of 30 s.

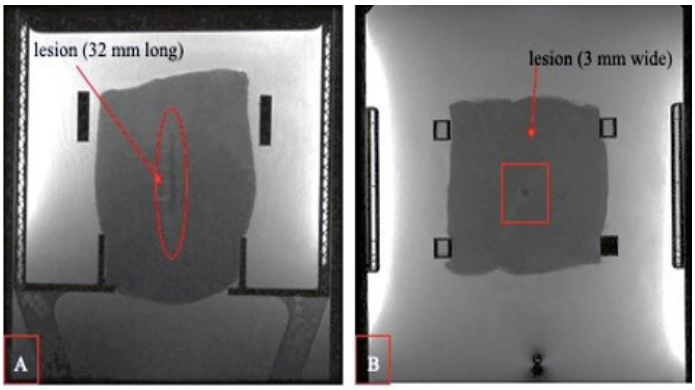

Figure 15: (A) High-resolution T2-W FSE MR image (axial plane), (B) High-resolution T2-W FSE MR image (coronal plane) obtained after applying acoustical power of 63 W, sonication time 30 s, frequency 1.1 MHz, d=50 mm, R=100 mm, focal depth= 45 mm.

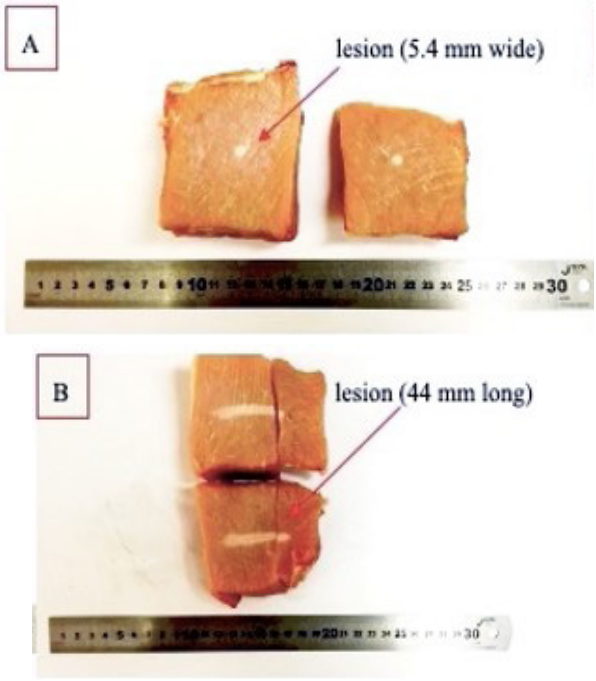

Figure 16: (A) Lesion formed at plane perpendicular to the beam, (B) Lesion formed at a plane parallel to the beam on ex vivo pork tissue resulting exposure at acoustical power of 63 W, sonication time 30 s, for the transducer with frequency 1.1 MHz, d=50 mm, R=100 mm, focal depth=45 mm.

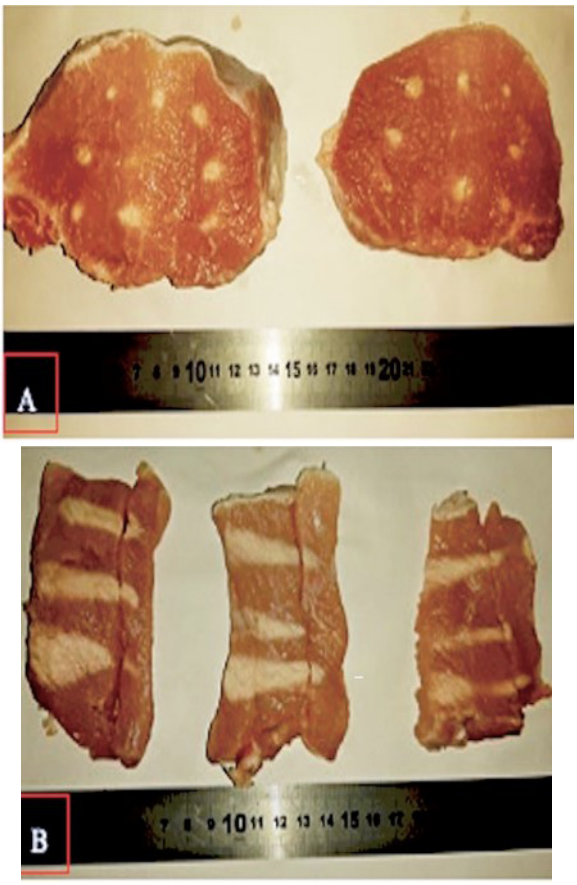

Figure 17: (A) Induced lesion in a plane perpendicular to the beam in ex-vivo pork tissue resulting from different sonication times, slice of the excised tissue at 40 mm (right) and its mirror image (left), (B)Induced lesion in a plane parallel to the beam in ex-vivo pork tissue resulting exposure at 74 W for different sonication times at focal depth of 4 cm using 1.1 MHz transducer.

Evaluation of the FUS system in *in vivo* rabbit model

Figure 18 shows an X-ray image taken for calculation of the thigh muscle. The surface area of the thigh was 20.6 cm^2 while the available surface area of all thighs was in the range 20.2-28.2 cm^2.

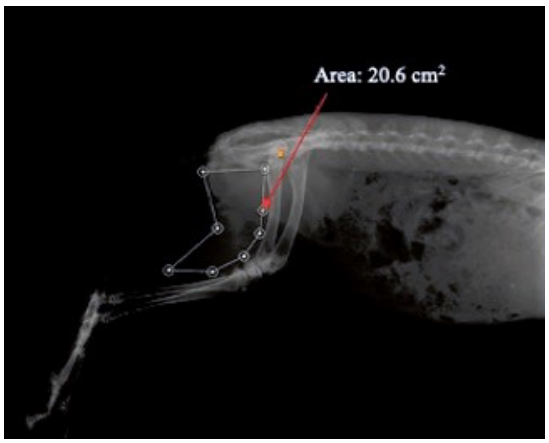

Figure 18: X-ray image of rabbit for calculation of thigh muscle area.

Movement of the robotic device was used for the formation of discrete lesions in a 1 x 3 array pattern with a 10 mm step size at a focal depth of 1 cm. Sonication of the right thigh was performed at acoustical power of 23 W for sonication times of 18 s, 40 s and 60 s. Figure 19A shows the formed lesions at a plane perpendicular to the beam. Lesion formed at 60 s had a diameter of 8 mm, lesion formed at 40 s had a diameter of 6 mm while lesion formed at 18 s had a diameter of 4 mm. Sonication was then performed at acoustical power of 15.6 W for a constant sonication time of 30 s. Figure 19B shows the formed lesions at a plane perpendicular to the beam after tissue dissection while Figure 19C shows one of the lesions formed at a plane parallel to the beam. The formed lesions had an average diameter of 5 mm and an average length of 10 mm.

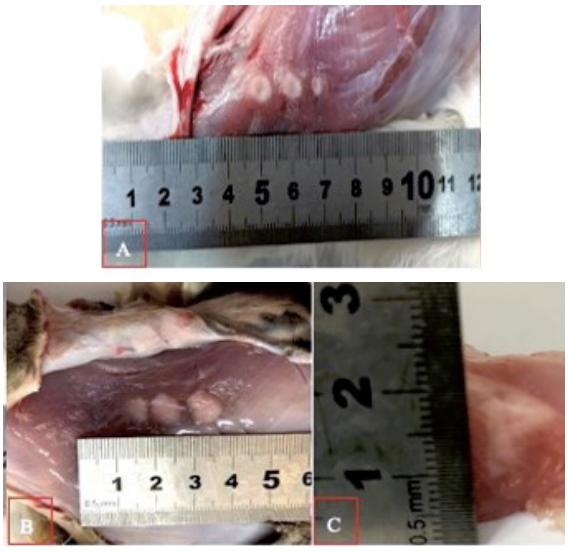

Figure 19: (A) Discrete lesions in a plane perpendicular to the beam in in vivo rabbit right thigh muscle resulting exposure at 23 W for sonication times of 60 s, 40 s and 18 s (from left to right) at focal depth of 1 cm, (B) Discrete lesions in plane perpendicular to the beam in in vivo rabbit right thigh muscle resulting exposure at 15.6 W for constant sonication time of 30 s, C) Induced lesion in plane parallel to the beam in in vivo rabbit thigh muscle resulting exposure at 15.6 W for sonication time of 30 s at focal depth of 1 cm.

Movement of the robotic device was then used for the formation of overlapping lesions in a 5 x 3 array pattern with a 3 mm step size at a focal depth of 1 cm. The right thigh muscle was sonicated using an acoustical power of 29.9 W for a sonication time of 30 s. Figure 20A shows the overlapping lesions formed on a plane perpendicular to the beam while figure 20B shows the lesions on a plane parallel to the beam. The lesion had a 17 x 15 mm^2 surface area and a length of 14 mm. An increased acoustical power of 74 W was then used for a sonication time of 7 s. Figure 20C shows the overlapping lesions formed on a plane perpendicular to the beam. The lesion had a 10 x 10 mm^2 surface area and a length of 8 mm.

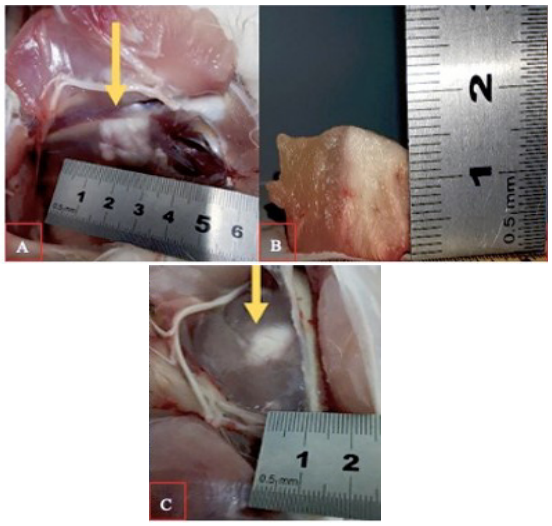

Figure 20: (A) Overlapping lesions in a plane perpendicular to the beam in in vivo rabbit right thigh muscle resulting exposure at 29.9 W for a sonication time of 30 s at focal depth of 1 cm, (B) Overlapping lesions in a plane parallel to the beam in in vivo rabbit right thigh muscle resulting exposure at 29.9 W for a sonication time of 30 s at focal depth of 1 cm, (C) Overlapping lesions in a plane perpendicular to the beam in in vivo rabbit thigh muscle resulting exposure at 74 W for a sonication time of 7 s at focal depth of 1 cm.

In vivo thigh ablation was performed inside the MRI environment using an acoustical power of 27 W for a sonication time of 40 s. Movement of the robotic device in a 3 x 3 array pattern was used for the formation of overlapping lesions. MR coronal images were acquired after sonication. Figure 21 shows the MR coronal image obtained after formation of the overlapping lesion.

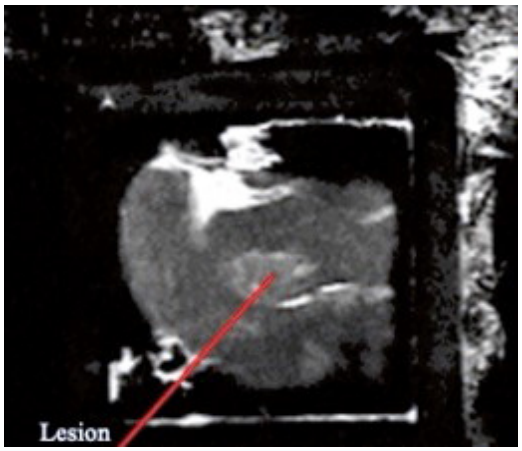

Figure 21: T2-W FRFSE MR image (coronal plane) acquired after in vivo sonication at acoustical power of 27 W for sonication time of 40 s with movement of the robotic device in a 3 x 3 grid with a 3 mm step size at 2 cm focal depth.

Discussion

An MRgFUS robotic device has been developed for preclinical use on small animals (mice, rats, rabbits, cats and small dogs). The robotic device offers movement in 4 DOF (3 linear and 1 angular) and can fit in any commercial MRI scanner up to 7 T. The motion accuracy of the positioning device was tested using a special structure attached to the robot and a digital caliper. Accuracy was tested for linear axes in distance increments of 1, 5 and 10 mm and 5 and 10 degrees for the angular axis. The intended distance was compared with the measured distance for forward and reverse direction (CW and CCW for Θ axis). Forward movement in the X axis for a 1 mm distance increment, has the greatest error (2.15 %) of all distance increments and directions of the X axis. The error for 5 mm distance increments in the reverse direction was larger than the forward direction whereas the error at 10 mm reverse direction was smaller than the forward direction. The error at the 5 mm step was almost five times larger than the error for 10 mm. Forward and reverse movement in the Y axis has resulted in greater error values than the X axis, with the 1 mm distance having the greatest. For 1 mm distance increment, forward and reverse direction accounted approximately for the same error (~6 %). Error in forward and reverse direction for each distance increment was approximately the same, with the error at the 5 mm step being larger than the 10 mm. Reverse movement in the Z axis at the 1 mm step, resulted in the smallest error (0.35 %) among all axes and step sizes. Forward direction at the same distance increment resulted in double the error value than reverse direction. For the 5 mm distance increment, forward and reverse direction accounted approximately for the same error (~2.1 %), making it the step with the highest error values among the Z axis. The average speed of motion was approximately the same for forward and reverse motion at each axis, with the speed at the Y axis being almost double than the X axis.

The speed of motion in the Z axis was approximately five times faster than the X axis and three times faster than the Y. Concerning angular motion, the error in the CW direction was higher than the error in the CCW direction, with smaller errors occurring at larger angle increments. The speed of motion in the Θ axis follows the pattern of the linear axes; approximately same speed between CW and CCW directions. It is concluded that the device is more accurate when larger distance increments are used in the X, Y and Θ axes, contrary to the Z where smaller distance steps induced smaller errors, and the motion is quicker at the Z axis. The accuracy of motion of 0.01-0.11 mm in the linear axes and 0.1-0.2 ° in the angular axis is making the robotic device highly accurate.

The spatial accuracy of the robotic device gives the ability of performing multiple sonications in a grid pattern. Sonications were performed on *ex vivo* porcine tissue in a 3 x 3 pattern proving excellent repeatability of the lesion formation. Lesion diameter and length was increasing with increasing sonication time. Lesions produced at 40 s had a cigar shaped, while lesions formed at 50 s had a tadpole shaped. This indicates a possible effect of cavitation in lesion formation.

The device was tested for MRI compatibility of the transducer and the robotic device by measuring the SNR for various activation conditions. The SNR of the transducer was measured using FSPGR whereas the SNR of the robotic device was measured using FRFSE, FSPGR and EPI. It was found to be decreasing with every activation condition and having minimal differences between EPI and FSPGR sequences. The MR compatibility of the

encoders and the motors provides the ability of obtaining thermal maps during sonications. This was proven by sonicating *ex vivo* porcine tissue at 63 W for 30 s and acquiring a thermal map during the sonication. The large temperature increase resulted in a cigar shaped lesion.

After indications that the FUS system can form reproducible and controllable lesions on excised tissue, its efficiency on ablating *in vivo* healthy rabbit muscle tissue was assessed. By adjusting the motion of the device in X and Y axes and the sonication parameters (power, time), discrete and overlapping lesions were formed on the rabbit thigh muscle tissue. Motion in the Z and Θ axes was not performed due to target size limitations (small thigh thickness). Higher sonication times at constant acoustical power of 23 W resulted in discrete lesions of greater diameter. Sonications performed at constant power of 15.6 W for constant sonication time of 30 s resulted in almost reproducible lesions, with two of the three lesions having the same diameter. By adjusting the step size between robotic movement, overlapping lesions were formed, having increased surface area at increasing energy (acoustical power x sonication time) values.

All discrete and overlapping lesions were formed at a 1 cm depth within the thigh, being in full accordance with the focal depth of the transducer. Therefore, this ensures that ablation was limited within the targeted muscle tissue without damaging in other areas. Monitoring of the vital signs of the rabbits was used to indicate any adverse effects. The rabbits remained in deep anesthesia until euthanasia with mild level severities experienced throughout the procedure.

The ability of the transducer to form normal shaped lesions, the excellent motion accuracy of the robotic device as well as its MRI compatibility are demonstrating the ability of using the device for MRgFUS for preclinical use. The *in vivo* ablations on rabbit muscle confirmed that the device is capable of inducing *in situ* tissue necrosis while the procedure does not compromise animal welfare and wellbeing. The device operates at 1.1 MHz and hence can be used for deep tissue ablation. Although its efficacy in ablating malignant tissues has not been verified, the experiments conclude that tumors larger than 1 cm can be precisely ablated in small animals. The use of a single element transducer is making the device easier to handle and more cost effective.

The propagation mechanism of the ultrasound requires attention near bones and nerves. The addition of an axis for angular movement allows ultrasound targeting in small angles, resulting in easy maneuvering of the ultrasonic beam near sensitive areas. The device has been designed to fit inside the MRI table, occupying minimal space. Its compact design and weight aid the easy transfer of the device. The motion range of the system can be used on animals with the future possibility of scaling up the design of the device for use on humans for abdominal targets. In our opinion, the proposed device will be more affordable and as effective as other similar devices for research purposes on small animals.

Acknowledgements

This work was supported by the Project FUSROBOT. The project was implemented within the framework of the Restart 2016-2020 program under the Research in Enterprises Action and funded by the Research Promotion Foundation of Cyprus (Project Code: ENTERPRISES/0618/0016).

References

1. Lynn JG, Zwemer RL, Chick AJ, Miller AE. A new method for the generation and use of focused ultrasound in experimental biology. J Gen Physiology. 1942; 26: 179-193.
2. Jolesz FA. MRI-guided focused ultrasound surgery. Annu Rev Med. 2009; 60: 417-430.
3. Blana A, Rogenhofer S, Ganzer R, Lunz JC, Schostak M, et al. Eight years' experience with high-intensity focused ultrasonography for treatment of localized prostate cancer. Urology. 2008; 72: 1329-1333.
4. Murat FJ, Poissonier L, Pricaz E, Rouviere O, Mege F, et al. Prognostic factors for salvage HIFU success after external beam radiation failure (EBRT) failure. Eur Urol Suppl. 2008; 7: 119.
5. Warmuth M, Johansson T, Mad P. Systematic review of the efficacy and safety of high- intensity focussed ultrasound for the primary and salvage treatment of prostate cancer. Eur Urol. 2010; 58: 803-815.
6. Yehezkeli O, Freundlich D, Magen N, Marantz C, Medan Y, et al. Mechanical positioner for MRI guided ultrasound therapy system. Inventors word intellectual property organization. INSIGHTEC-TXSONICSLTD. Assignee. WO0209812A1. 2002.
7. Napoli A, Anzidei M, De Nunzio C, Cartocci G, Panebianco V, et al. Real-time Magnetic Resonance–guided High-intensity Focused Ultrasound Focal Therapy for Localised Prostate Cancer: Preliminary Experience. European Urology. 2013; 63: 395-398.
8. Khiat A, Gianfelice D, Amara M, Boulanger Y. Influence of post-treatment delay on the evaluation of the response to focused ultrasound surgery of breast cancer by dynamic contrast enhanced MRI. The British Journal of Radiology. 2006; 79: 308-314.
9. Kopelman D, Inbar Y, Hanannel A, Dank G, Freundlic D, et al. Magnetic resonance-guided focused ultrasound surgery (MRgFUS). Four ablation treatments of a single canine hepatocellular adenoma. HPB. 2006; 8: 292-298.
10. Catane R, Beck A, Inbar Y, Rabin T, Shabshin N, et al. MR-guided Focused Ultrasound Surgery (MRgFUS) for the Palliation of Pain in Patients with Bone Metastases-Preliminary Clinical Experience. Annals of Oncology. 2007; 18: 163-167.
11. Lipsman N, Schwartz M, Huang Y, Lee L, Sanka T, et al. MR-guided focused ultrasound thalamotomy for essential tremor: a proof-of-concept study. Lancet Neurol. 2013; 12: 462-468.
12. Chopra R, Curiel L, Staruch R, Morrison L, Hynynen K. An MRI-compatible system for focused ultrasound experiments in small animal models. Med Phys. 2009; 36: 1867-1874.
13. Image Guided Therapy. [http://www.imageguidedtherapy.com]
14. Krafft A, Jenne J, Maier F, Stafford J, Huber P, et al. A long arm for ultrasound: a combined robotic focused ultrasound setup for magnetic resonance-guided focused ultrasound surgery. Med Phys. 2010; 37: 2380-2393.
15. FUS Instruments. [https://www.fusinstruments.com/products]
16. Alpinion. [http://www.alpinion.com/web/therapeutic/ vifu_2000.asp]
17. TooSonix system. One-R system description. [https://www.toosonix.com]
18. Verasonics. HIFUPlex system description. [https://verasonics.com/hifuplex-options/]

19. The Association of Electrical and Medical Imaging Equipment Manufacturers. Determination of Signal-to-Noise-Ratio (SNR) in Diagnostic Magnetic Resonance Imaging. NEMA Standard Publication MS 1. 2008.

20. Menikou G, Damianou C. Acoustic and thermal characterization of agar-based phantoms used for evaluating focused ultrasound exposures. Journal of Therapeutic Ultrasound. 2017: 5.